Research Article Vol. 30, No. 1 / 3 Jan 2022 / Optics Express 414
Optics EXPRESS

Engineered fluidic device to achieve multiplexed monitoring of cell cultures with digital holographic microscopy

ERIK BÉLANGER,[1,2,7,8] CARINE BENADIBA,[3,7] ÉMILE RIOUX-PELLERIN,[1] FRÉDÉRIC BECQ,[4] PASCAL JOURDAIN,[3] AND PIERRE MARQUET[1,3,5,6,9]

[1]*Centre de recherche CERVO, Québec, Canada*
[2]*Département de physique, de génie physique et d'optique, Université Laval, Québec, Canada*
[3]*Unité mixte internationale en neurodéveloppement et psychiatrie de l'enfant, Centre des neurosciences psychiatriques, Département de psychiatrie, Centre hospitalier universitaire vaudois, Université de Lausanne, Lausanne, Suisse, Université Laval, Québec, Canada*
[4]*Laboratoire signalisation et transports ioniques membranaires, Université de Poitiers, Poitiers, France*
[5]*Centre d'optique, photonique et laser, Québec, Canada*
[6]*Département de psychiatrie et neurosciences, Université Laval, Québec, Canada*
[7]*These authors contributed equally*
[8]*erik.belanger.1@ulaval.ca*
[9]*pierre.marquet@neuro.ulaval.ca*

Abstract: We present a low-cost, 3D-printed, and biocompatible fluidic device, engineered to produce laminar and homogeneous flow over a large field-of-view. Such a fluidic device allows us to perform multiplexed temporal monitoring of cell cultures compatible with the use of various pharmacological protocols. Therefore, specific properties of each of the observed cell cultures can be discriminated simultaneously during the same experiment. This was illustrated by monitoring the agonists-mediated cellular responses, with digital holographic microscopy, of four different cell culture models of cystic fibrosis. Quantitatively speaking, this multiplexed approach provides a time saving factor of around four to reveal specific cellular features.

1. Introduction

The field of live-cell quantitative-phase imaging (QPI) has experienced a dramatic growth these last two decades [1]. Among the many QPI approaches developed, digital holographic microscopy (DHM), thanks to its accurate quantitative-phase signal (QPS), has enabled to achieve very appealing applications including cell culture inspection [2], automated cell counting, recognition, and classification for diagnostic purpose [3] with the use of machine learning approaches [4]. Furthermore, DHM has successfully monitor the activity of cation chloride co-transporters [5] and chloride channel receptors including the epithelial chloride channel cystic fibrosis transmembrane conductance regulator (CFTR) [6] as well as their modulation by specific agonists and antagonists [7].

A crucial point to successfully perform live-cell experiments is to have an imaging chamber which allows maintaining cells in a healthy state while being compatible with the requirements of the experimental protocols. To this end, multi-well plates are widely used in high-throughput screening (HTS) approaches aiming at rapidly testing the ability of thousands or even more compounds to act on a previously identified target [8–10]. Such HTS techniques effectively capture many cellular features on a large scale and in an automated manner at specific time points. However, deciphering in details cellular mechanisms or processes as well as their interrelationships requires the use of more complex protocols especially pharmacological ones,

#444701 https://doi.org/10.1364/OE.444701
Journal © 2022 Received 1 Oct 2021; revised 12 Nov 2021; accepted 13 Nov 2021; published 21 Dec 2021

Optics EXPRESS

such as the application of several substances in a transient, concomitant, or sequential manner. Achieving such accurate and well-controlled perfusion sequences of different drugs requires perfusion chambers that can offer laminar fluid flows. Indeed, flow disturbances are prone to swirls that trap the liquid (and the pharmacological agent), create counter-current flows, or eddies and preclude rapid rinsing [11,12]. Over the years, a wide range of perfusion chambers from simple to more sophisticated, commercial to home-built in open or closed configurations, have become available. About most commercial perfusion chambers, the flow pattern is either not provided or not suitable for a uniform delivery of liquid, in both space and time. Indeed, the fluid flow is usually disturbed due to the presence of changes in ducting diameter and plumbing accessories (valves, bends, and other fittings). Furthermore, validating specific cell responses, *i.e.* to assess its reproducibility, requires considering a representative cell sample, which means having to repeat the experiments several times to ensure that a sufficiently large number of cells from different coverslips are analyzed. This repetition of experiments becomes particularly time-consuming when it is wanted to characterize several different cell types. On the other hand, the recent advance of general-public 3D printers, namely fused deposition modeling, offers a unique opportunity to easily design and fabricate customized live-cell imaging chambers in a cost-effective manner [12–15]. In one embodiment, a fluidic device with a one-step diffuser, which consequently has a small field-of-view in the form of a slit is reported. This specific geometry, characterized by a low dead volume, is therefore ideal for fast rinsing. Consequently, using this fluidic device in conjunction with a two-liquid decoupling procedure, absolute cell volume measurement with an accuracy of the order of 50 fL at the single-cell level was demonstrated [12].

Aiming at different applications and keeping in mind the requirements related to both fluidics and result reproducibility, we have presently developed a low-cost, large field-of-view, 3D-printed fluidic device with a tailored geometry enabling a laminar flow, homogeneous over a significant part of its extensive imaging cavity, thus offering the possibility to perform multiplexing, *i.e.* being able to record at once the responses of several cell cultures on which the same experimental protocol is applied simultaneously. After having presented the fluidic device, especially its conception, making and characteristics, its multiplexing capabilities will be stressed through a biological application involving four different Chinese hamster ovary (CHO) cell lines transfected (or not) with human gene variants of CFTR protein. CFTR is a multi-functional protein that constitutes a Cl^- channel and has a regulatory function on other Cl^- channels. It is well known that these different gene variant of CFTR drastically affect the cellular Cl^- permeability [16]. On the other hand, DHM, as previously mentioned, is a technique that can accurately measure the activity of specific Cl^- channels including CFTR [6]. Therefore, a multiplexed monitoring, that provides at once the QPS measurements from each of these four different CHO cultures when simultaneously stimulated by known CFTR agonists, is presented.

2. Materials and methods

2.1. Computational fluid dynamics

Top view, two-dimensional and steady-state flow simulations of the imaging cavity are made with the computational fluid dynamics (CFD) module of COMSOL Multiphysics (5.3a, COMSOL). The details of the simulations are as follows, in line with chapters two and three of Ref. [17]. The entrance lengths are derived from the Reynolds number expression in circular pipes obtaining values varying from 1 to 2 mm depending on the inflow specified (fully developed inflow). The flow rate to velocity conversion is achieved using an entrance height equal to the maximum height of the duct, notably 1.6 mm. Steady-state numerical solutions of the Navier-Stokes equations are computed for flow rates values from 1.0 to 2.4 mL/min [12].

Additionally, time-dependent simulations of species concentration are made at flow rates of 1.0, 1.5, and 2.0 mL/min to assess the diffusion dynamics in the fluidic device. To do that,

Optics EXPRESS

the dilute species transport module is coupled to laminar flow simulations enabling flow field numerical solutions to calculate solute transport via convection, according to chapter eight of Ref. [17]. More specifically, at the initial time point the duct is prefilled with pure solvent, while a species concentration of 100 mM is the solute at the inlet. For all simulations, the walls are attributed a no-slip boundary condition.

2.2. Micro-particle image velocimetry

Flow in the fluidic device is assessed experimentally with micro-particle image velocimetry (μPIV). Polyethylene 30-μm microbeads of 1.00 ± 0.01 g/cm^3 density (VIOPMS-1.00 27-32um, Copsheric LLC) are coated with TWEEN 80 (Cospheric LLC) to reduce hydrophobicity according to the provider's protocol. A small amount (200 μL) of the resulting coated microbeads are then suspended in 10 mL of deionized water. With a syringe pump (Legato 185, KD Scientific) and silicon tubing (OF-06424-59, Cole-Parmer), the microbeads solution is perfused through the fluidic device. Videos of the microbeads solution flowing through the imaging cavity are taken using a vertical imaging setup comprised of a vision camera (Grasshopper3, FLIR) equipped with a monochrome 2.3-megapixel Sony IMX174 CMOS sensor with a pixel size of 5.86 μm. The setup also contains a magnification zoom lens system (MVL-7000, NAVITAR), more precisely a macro lens with variable focal length from 18 to 108 mm and a magnification of 1.1X at its minimum working distance of 130 mm. The microbeads trajectories are recorded at flow rates ranging from 1.0 to 2.4 mL/min with an increment of 0.2 mL/min. The videos frame rates vary from 50 to 163 fps, proportionally to the flow rates. Beads trajectories are traced in videos using the automatic tracking TrackMate plug-in (V5.2.0, NIH) [18] in ImageJ (v1.52p, NIH) to obtain the experimental streamlines.

2.3. Neuronal viability assay

Rat primary neurons are grown on a total of 11 coverslips [19]. Five control and six experimental coverslips are mounted in a commercially available perfusion chamber (CF-T18, Live Cell Instrument) equipped with a circular gasket (CF-T18-Z3, Live Cell Instrument) and in the fluidic device for viability assessment, respectively. Coverslips are perfused for 30 min in a HEPES-buffered physiological medium containing (in mM) 100 NaCl, 5.4 KCl, 1.8 $CaCl_2$, 0.8 $MgCl_2$, 0.9 NaH_2PO_4, 10 HEPES, and 5 D-glucose at a pH of 7.4 (all from Sigma). All coverslips are then stained for 3 min with a 0.04% Trypan Blue solution (MT25900CI, Fisher Scientific). Stained cells are imaged with a 20X microscope objective having a free working distance of 3.1 mm and a numerical aperture (NA) of 0.40 (PL FL LWD PH, Invitrogen) by a transmitted-light microscope (EVOS FL, Invitrogen). Images are separated in function of the section wherein they are taken (top, center, and bottom of the imaging cavity) with an average of 11 acquisitions per region per coverslip. Dead and live cells are identified by their staining, or lack thereof, and manually counted with ImageJ (v1.52p, NIH).

2.4. CHO cells

Four different CHO cell lines are used. The first one corresponds to CHO-K1, a cell type that does not express the CFTR protein (native CHO). The second line expresses a CFTR functional form (CHO-CFTR) while the third and fourth lines express two CFTR isoforms known to lead to a Cl^- cellular impermeability (CFTR-ΔF508 and CFTR-G551D). Specifically, CHO-ΔF508 expresses CFTR protein with phenylalanine deletion in position 508 (prevalence up to 90%) and CHO-G551D expresses CFTR protein with a substitution of glycine by aspartate at position 551 (prevalence around 4%). The detailed culture procedure for CHO cells, non-transfected (K1) and stably transfected with wild-type CFTR or other CFTR variants isoforms (ΔF508 and G551D), is described in [20,21]. Briefly, cells, incubated at 37°C with 5% CO_2, are maintained in α-MEM (32561, Gibco), which contains 7% fetal calf serum (2-01F30-I, Bioconcept), 100

Optics EXPRESS

U/mL penicillin/streptomycin (15140122, ThermoFisher) and 200 µM, 100 µM, 20 µM or 0 µM methotrexate (A6770, Sigma) for CHO-ΔF508, CHO-CFTR, CHO-G551D and CHO-K1 respectively. The 4-well insert (80466, Ibidi) is deposited on a 20-mm coverslip (10.0360.58, Huberlab) coated the day before the experiment with poly-L-ornithine at 25 µg/mL (P3655, Sigma). Then, each CHO cell type is passed with Trypsin-EDTA (5-51F00-H, Bioconcept) after a PBS wash, counted, and individually plated into a given well delimited by the insert at a density of 10^3 cells per cm^2. Before performing experiments, cells adhered overnight in separate culture media, thus creating four independent cell cultures.

2.5. CHO experimental stimulation

The cell culture medium is replaced by the perfusion medium at room temperature 30 min before the start of the experiments. The perfusion medium contains (in mM) 140 NaCl, 3 KCl, 5 D-glucose, 10 HEPES, 3 $CaCl_2$ and 2 $MgCl_2$ (pH 7.3 with NaOH, all from Sigma). Then, the 4-well insert is carefully removed from the coverslip and mounted in the fluidic device and then connected to a gravity perfusion system. The perfusion system is composed of 60 cc syringes (4617509F, B.Braun) disposed on a post at a given height (defined to obtain the desired flow rate). The syringes are linked to electronic pinch valves (ValveBank8, AutoMate Scientific) with 1/32-inch inner diameter C-Flex tubing (W464-0166, Warner Instruments) itself connected to a PTFE micro-manifold 8-into-1 (05-08, AutoMate Scientific). The fluidic device is connected to the micro-manifold by a 1/16-inch inner diameter Tygon tubing (W464-0167, Warner Instruments). The flow rate is adjusted to 1.8 mL/min. The tubing upstream and downstream of the fluidic device should be secured to avoid the propagation of any potential vibration. When the tubing is correctly connected to the fluidic device, cultures are then perfused during a minimal period of 10 min to obtain a stable readout. Once obtained, experiments are started according to following procedure: 5 min of baseline - 5 min application of 8-Bromoadenosine 3',5'-cyclic monophosphate (8Br-cAMP) at 1 mM (B7880, Sigma) or forskolin at 10 µM (F6886, Sigma) - 15 min of rinsing. 8BR-cAMP and forskolin are known to induce, through different mechanisms, an opening of the CFTR channel's gate [20,21]. Specifically, forskolin is a direct activator of the adenylate cyclase, while 8BR-cAMP is a cell-permeable cAMP analog, known to constitutively activate the protein kinase A.

2.6. Digital holographic microscopy

The commercial digital holographic microscope (T-1003, Lyncée Tec) works by splitting a coherent light source in two: the object beam which passes through the sample, and the reference beam. The microscope objective, located in the object arm, has a magnification of 2.5X with a working distance of 11.3 mm and a NA of 0.07 (HCX FL PLAN, Leica). The resulting field-of-view of 3-4 mm^2 allows to cover, at once, the central region of the coverslip containing the four cell cultures. At the exit of the interferometer, the two beams interfere producing a hologram in the camera plane. The configuration is an off-axis geometry, meaning that a small angle is introduced between the direction of propagation of the object and reference waves. A CCD camera (eco285MVGE, SVS-Vistek) equipped with a monochrome 1.4-megapixel Sony ICX285AL sensor and a pixel size of 6.45 µm captured the holograms. Throughout experiments, holograms are acquired at a frequency of 0.1 Hz. Using proprietary software (Koala, Lyncée Tec), holograms are reconstructed to obtain quantitative-phase images [22]. Each single cell temporal trace corresponds to the QPS averaged over 30% of the cell body from times series of quantitative-phase images. For each cell temporal trace, the QPS surrounding background (an empty region around the cell) is used as a reference to suppress potential mechanical and thermal drifts [23].

Optics EXPRESS

3. Results and discussion

3.1. Description of the fluidic device

Figure 1(A) shows an exploded view of the fluidic device, elaborated with SolidWorks (2018, Dassault Systèmes), that is developed based on the results of numerical simulations (see Section 2.1). The fluidic device is composed of two main parts, the sample holder (diameter of 28 mm, thickness of 1.7 mm), and the mounts (lid and base) (Figs. 1(A)-(B)). The imaging cavity is then closed by two glass coverslips, the sample coverslip (covered with the cells) on the bottom and a coverslip sealed on top which acts as a transparent window closing the imaging cavity. Magnets on each of the two mounts allow to hold together the distinct parts of the fluidic device. For sizing purposes, an assembled fluidic device (top) and a sample holder (bottom) are shown next to a metric ruler in Fig. 1(B). Figures 1(C)-(D) present two cross-sections of the sample holder with all the dimensions listed. The imaging cavity is elliptically shaped, 13 by 8 mm with an area of 81.7 mm^2. The fluidic device is connected to metal microtubes at both sides of the duct. On the other hand, the plastic used must be biocompatible especially when there is a close contact with biological samples, as for the sample holder. The choice is turned towards a PETG plastic which has a medical grade certification (ISO 10993). Concerning the mounts, a PLA plastic is chosen for easier printing.

3.2. Realization of the fluidic device

The model files are sliced into layers with Cura (3.6, Ultimaker) before they are produced using a 3D printer (2 Extended+, Ultimaker). PETG plastic (guidel!ine, taulman3D) and a 0.25-mm nozzle (M2551-025, Micro Swiss) are used to print the sample holder with full infill and 30% infill overlap, helping to prevent most leaks. PLA plastic (PLA+, eSUN) and a 0.4-mm nozzle (M2551-04, Micro Swiss) are used to print the lid and base with 20% infill and 30% infill overlap. Rare earth magnets (5862K961, McMaster-Carr) are glued (5551T72, McMaster-Carr) in the four open sockets in both the top and bottom mounts, with opposite polarities facing up. Metal microtubes (304F10032X006SL, MicroGroup) of about 2.5 cm in length with respective inner and outer diameters of 0.4 mm and 0.8 mm are glued in each side of the sample holder. To ensure complete water tightness, the sample holder is treated with acetone (270725, Sigma-Aldrich) as described elsewhere [24]. Briefly, the top of the sample holder is exposed to acetone vapors for around 15 min and an 18-mm coverslip (GG18-1.5-PDL, Neuvitro) is immediately pressed in the inset. This step fixes the top coverslip in place, without the use of grease. If the top coverslip comes off with use, grease can be utilized to secure it. Furthermore, it is worthwhile to mention that such a 3D printing fabrication technique is quite easy to implement and very flexible. A new end-user can easily replicate the fluidic device, replace a component or modify the design. The fabrication cost of the entire fluidic device, including the plastic material, is about 13 USD. The technical drawings will be available upon request to the corresponding author.

3.3. Use of the fluidic device

To use the fluidic device, the sample coverslip is placed in the center of the base, on top of a previously cut parafilm O-ring gasket (M, BEMIS). To promote water/air tightness, a new parafilm gasket must be placed beneath the bottom coverslip at each use. A drop of cell medium is placed on the sample, preventing cells from air-drying. The sample holder, turned upside down, is filled slowly with medium using a small syringe and tubing. Keeping the syringe attached, the sample holder is flipped on the bottom coverslip, closing the imaging cavity. The lid is then placed on top delicately to avoid breaking the coverslips with the force of the magnets. Those magnets provide enough force to resist to internal water pressure, in no way limiting the flow rate that can be used. Based on a daily usage in the laboratory, the lifetime of the sample holder is

Optics EXPRESS

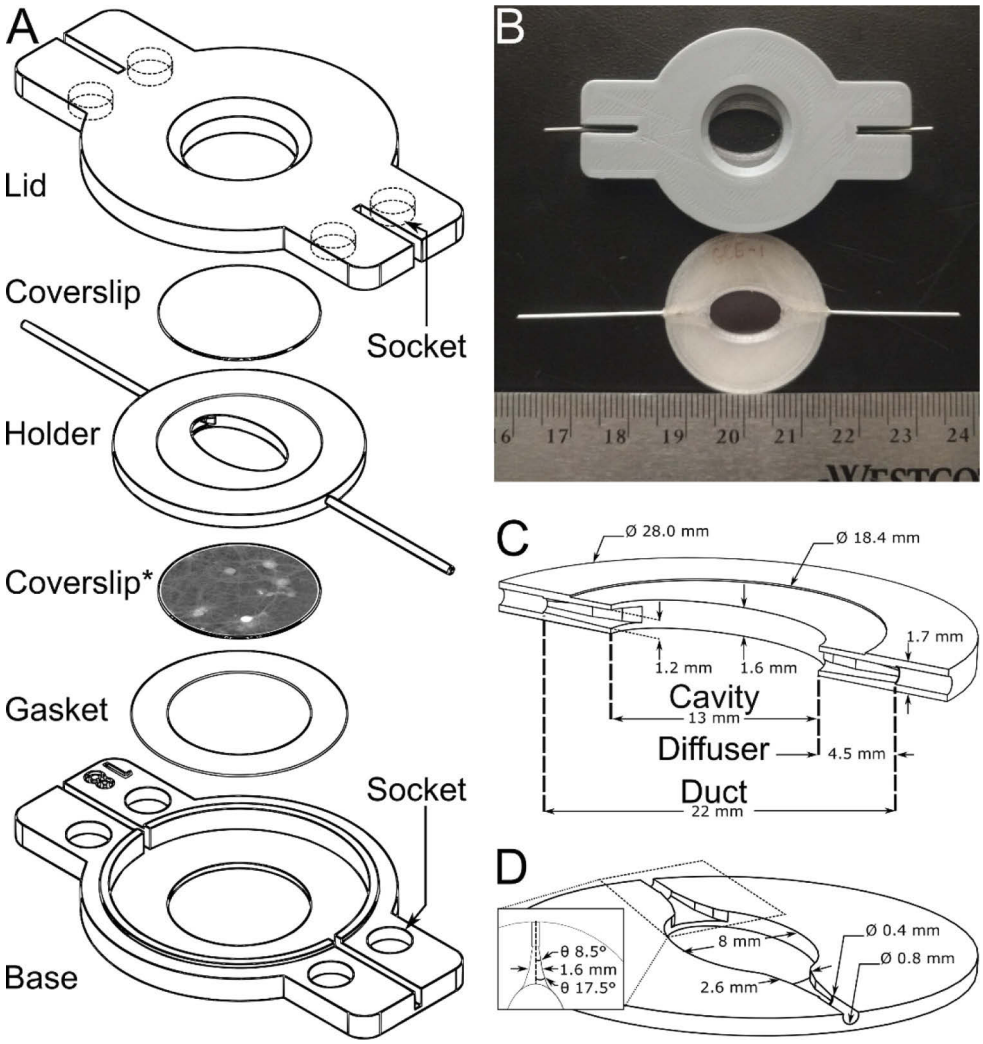

Fig. 1. Mechanical design. (A) An exploded view representing the fluidic device and detailing its constituents, including a schematic representation of the cell culture on the bottom coverslip indicated by an asterisk. (B) Photograph showing the assembled fluidic device (top) and a sample holder (bottom) as well as a ruler, for sizing purposes. (C, D) Drawings of the sample holder showing, respectively, a vertical and horizontal cross-section of the duct highlighting the diffusers and the imaging cavity. (D, Inset) Diagram emphasizing the location and angles of the diffusers. Magnets (not shown) are glued in sockets.

around 3 months after which leaks may occur or a degradation of the fluidic performances may be experienced.

3.4. Conception of the fluidic device with computational fluid dynamics

As previously mentioned, to design a fluidic device that allows to maintain a laminar flow, in a reasonable range of perfusion rates, to perform controlled perfusion sequences of different drugs, is needed. Moreover, such a flow must also be as homogeneous as possible over relatively large field-of-view (typically 3-4 mm^2) corresponding to low-magnification microscope objectives (here 2.5x), normally used to analyze cellular responses from many cells at a time (usually a

Optics EXPRESS

thousand). It is well known from fluid mechanics that sudden changes in cross-sections, such as at the interface between the inlet pipe and the entrance of the imaging cavity (as well as at the junction of the exit of the imaging cavity and the outlet pipe), promote instability in the flow field, creating a separation of the flow and inducing backflows or eddies a phenomenon usually called minor losses. To illustrate this behavior, a time-lapse of a µPIV experiment in a commercial perfusion chamber at a flow rate of 1.8 mL/min showing the vast spatial extent of the eddies (in this specific case, up to 75% of the flow field) is shown in Visualization 1 (flow goes from left to right, scale bar indicates 2 mm), therefore confirming the inappropriateness of such a chamber for multiplexed monitoring of cell cultures. This phenomenon can, however, be minimized if the expansion (contraction) of the diffuser (nozzle) is made gradual.

Since then, numerical simulations have focused on the geometry of the diffuser (the nozzle geometry is identical which allows the holder to be used in either direction) to preserve as well as possible the flow laminarity. First, it was hinted previously, the use of a diffuser with a full-angle around 8° is preferable to gradually transition from one cross-section to another [11]. Moreover, it is important to consider the junction angles at the entrance and exit of the imaging cavity. Indeed, in practice, a rectangular cavity leads to small junction angles creating an extremely reduced field-of-view [12]. Alternatively, a circular cavity usually results in an appreciable field-of-view, but as the junction angle is too large, it creates eddies. Therefore, an elliptical cavity elongated in the flow direction is an effective compromise both in terms of obtaining a large field-of-view and the reduction of the junction angle prevents the creation of eddies.

Based on these considerations, simulations were performed and lead to a geometry which includes a two-step diffuser with two different opening angles (Figs. 1(C)-(D)). The first half-angle of the diffuser is 8.5°. This diffuser step transitions gradually over 2.6 mm from a circular to a rectangular cross-section of 1.6 mm in width. Then, the opening half-angle switches to 17.5° with a relative angle between the two steps of 9° and extend over 1-mm distance. This two-step opening, emphasized in the inset of Fig. 1(D), allows to increase the flow rate while avoiding a separation of the flow which creates backflows. At 2.6 mm from the inlet, the transition to the ellipse is made with a rounded chamfer using a junction angle allowing gradual docking to the imaging cavity without compromising the laminarity of the flow for a larger imageable surface. The duct also enlarges slowly on the vertical axis, reaching a height of 1.2 mm at the entrance of the imaging cavity.

Once the fluidic device was built according to the results of the simulations, its flow properties were assessed. For this purpose, streamlines, experimentally measured with µPIV, were compared with 2D simulations presenting a top-view of the duct. Figure 2 shows simulated and experimental streamlines at 6 different flow rates for the entire elliptically shaped imaging cavity (13 by 8 mm). At low flow rates, in agreement with the simulation, no separation between streamlines (Figs. 2(A1)-(A2) and Figs. 2(B1)-(B2)) are observed, the flow remains laminar throughout the imaging cavity. At 1.8 mL/min (Figs. 2(C1)-(C2)), backflows start to appear in the simulation, grow slightly as flow rate increases (Figs. 2(D1)-(D2)) and eddies are revealed experimentally with µPIV when the flow rate is augmented to 2.2 mL/min (Figs. 2(E1)-(E2) and Figs. 2(F1)-(F2)) or more. This laminar behavior contrasts greatly with that of a commercial perfusion chamber reported in Visualization 1. Interestingly, both simulations and experimental measurements show that for values up to 2.4 mL/min the center of the fluidic device still exhibits no backflows or eddies, a crucial point for several other applications demanding, particularly, high flow rates such as flow-induced alignment of epithelial cells.

To facilitate the comparison between simulation results and experimental measurements, a comprehensive ratio, namely the normalized laminar area, defined as the portion of the imaging cavity that remains laminar divided by the total area, is plotted as a function of the flow rate (Fig. 3). Consistently, the flow remains laminar, up to a critical value at which the ratio shows a quite linear decrease, reflecting a shortening of the proportion of the imaging cavity along which

Optics EXPRESS

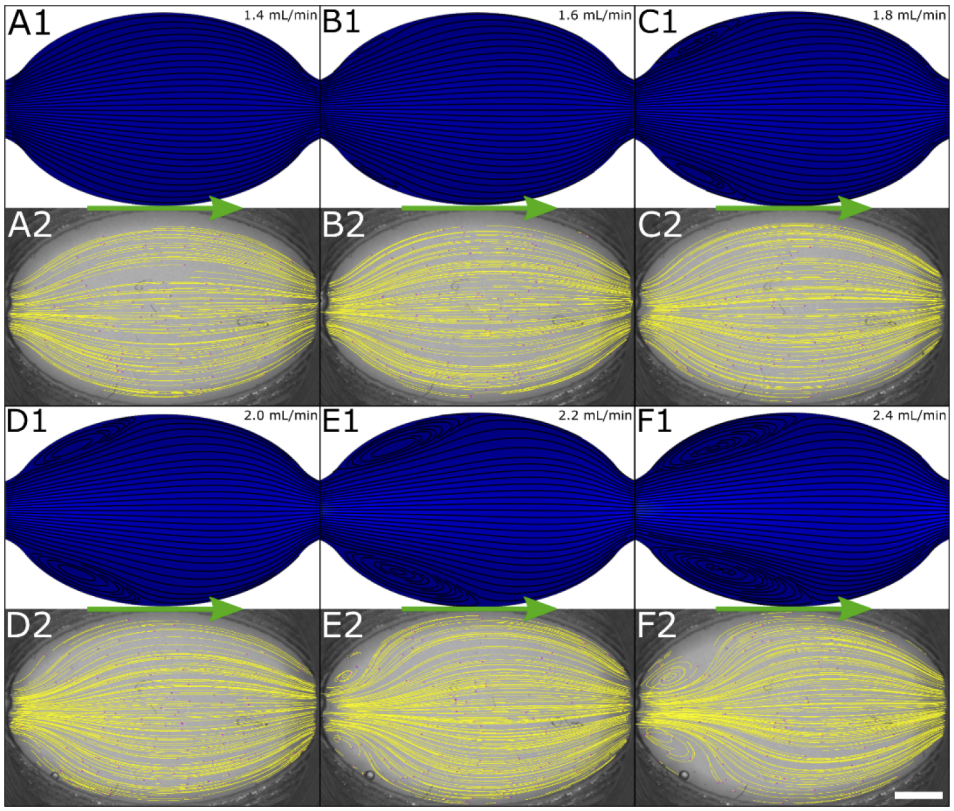

Fig. 2. Laminar and homogeneous flow. (A)-(F) Comparison of CFD simulation (top, 1) and experimental µPIV (bottom, 2) of the fluidic device at six different flow rates: 1.4, 1.6, 1.8, 2.0, 2.2, and 2.4 mL/min, respectively. Arrows specify the flow direction, scale bar indicates 2 mm.

the flow laminarity is maintained. Such behavior is observed with both simulations and µPIV measurements but occur for slightly different breakpoints. The decrease obtained experimentally starts from 2.2 mL/min against 1.6 mL/min in case of simulations. Such differences could be due that the microbeads do not have the same density as water or thermal expansion modifying ducting dimensions.

To mimic a pharmacological stimulation, a transition period in the fluidic device resulting from a sequential perfusion of two solutions is simulated, the first one corresponding to the basal solution and the second one to the stimulating solution, *i.e.* the one that additionally contains an active pharmacological substance (the solute) at a determined concentration. More specifically, the perfusion of a solution containing a given solute concentration (the inflow of the stimulating solution) into the imaging cavity that was pre-filled with the pure solvent (the basal solution) is simulated (see Section 2.1). At flow rates of 1.0 and 1.5 mL/min the simulations do not exhibit any unmixed regions (see Visualization 2 and Visualization 3). The relative solute concentration is approaching 100% (*i.e.* the solute concentration of the inflow solution) in the center of the imaging cavity in about 8 or 4 s at 1.0 and 1.5 mL/min, respectively. Because of the typical no-slip boundary condition of the flow, a thin film adjacent to the sides of the imaging cavity stagnates at 0% during the total duration of the simulation (30 s). At 2.0 mL/min, eddies occur with their consequences *i.e.* two small regions on either side of the entrance persist with a relative solute concentration lower than that of the stimulating solution, and this in a prolonged period

Optics EXPRESS

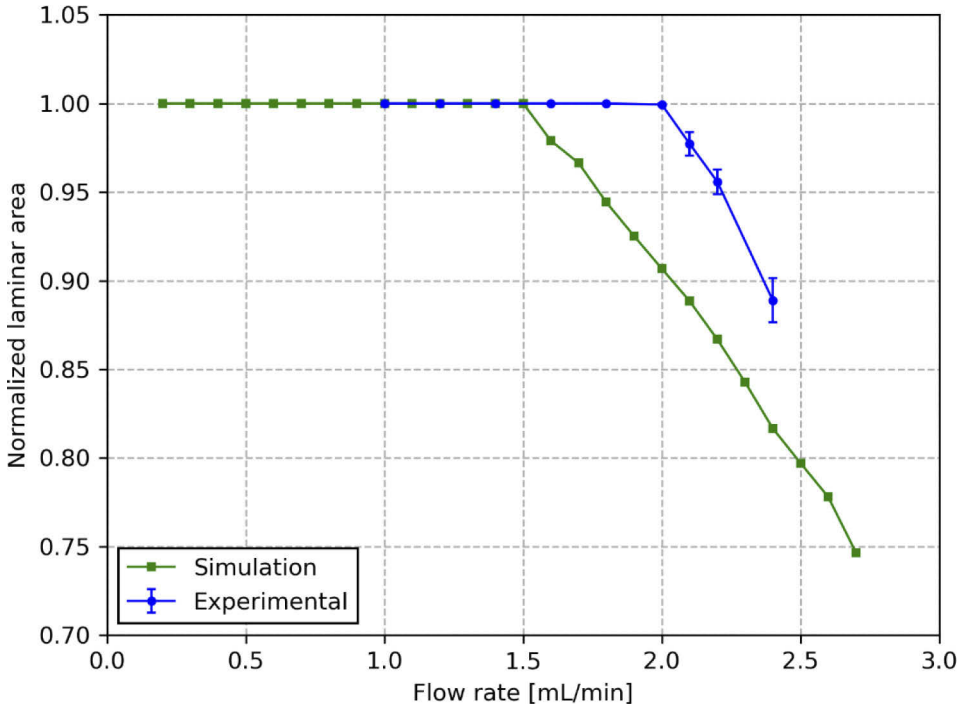

Fig. 3. Laminar area. Normalized laminar area of the fluidic device as a function of flow rate obtained with CFD simulations (green line, squares) and experimental μPIV (blue line, circles).

(see Visualization 4). Based on these results and to maintain a laminar flow as homogeneous as possible over a large part of the imaging cavity, the subsequent experimentations are performed with a flow rate around 1.8 mL/min, which represents a good compromise to promote fast drug delivery without disturbances.

3.5. Biocompatibility assessment

Biocompatibility is essential for a fluidic device. While the sample holder is made with medical grade certified material, it is judged necessary to perform a neuronal viability assay for confirmation. According to the protocol described in Section 2.3, the viability test is performed on neurons, a type of cell well-known for its high sensitivity to environmental conditions. For comparison purposes, experiments are performed both in a commercially available perfusion chamber (Section 2.3) and in the fluidic device. Figure 4 shows the percentage of living neurons after the 30-minute perfusion in both conditions. The mean viability rates across all regions of the coverslip are $70.95 \pm 6.99\%$ ($n_{cell} = 18064$) for the commercial chamber and $77.33 \pm 7.08\%$ ($n_{cell} = 22254$) for the fluidic device, without showing any statistically significant difference (Student's t-test, $p \geq 0.05$). These viability rates are excellent considering the experimental stress that cells undergo during samples mounting in the commercial chamber and fluidic device. Moreover, the neuronal viability rates across different coverslip regions of the fluidic device (top = $75.94 \pm 7.88\%$, $n_{cell} = 7215$; middle = $81.07 \pm 7.69\%$, $n_{cell} = 7979$; and bottom = $74.99 \pm 8.46\%$, $n_{cell} = 7060$) do not differ significantly from each other (Student's t-test, $p \geq 0.05$). This spatial homogeneity feature, reflecting that the distinct locations of the coverslip correspond to similar environmental conditions, is particularly important to exploit the multiplexing capabilities of the fluidic device.

Optics EXPRESS

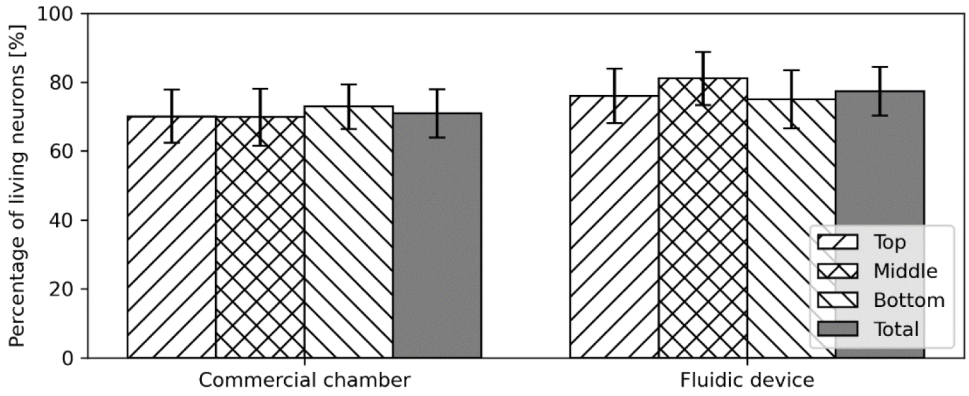

Fig. 4. Biocompatibility assessment. Average percentage of living neurons per region and in total observed in a commercial perfusion chamber (Section 2.3) and the fluidic device.

3.6. Validation of the fluidic device multiplexing capability

To illustrate the multiplexing capability of the fluidic device, pharmacological experiments, involving 8Br-cAMP and forskolin (known to induce an opening of the CFTR channel's gate) performed simultaneously on the four CHO cell lines, are presented. The schematics, in Figs. 5(A1)-(A3), illustrate the use of the 4-well insert to create independent cell cultures as well as resulting arrangement inside the fluidic device. The use of a 2.5x-microscope objective, providing a field-of-view of 3-4 mm^2, allows to visualize in one shot between 200 and 300 cells in each of the four cultures (Fig. 5(A4)). Thus, according to Section 2.6, the reconstruction and analysis of a single hologram provides the QPS corresponding to about 50 cells, randomly selected, for each of the four cell cultures (Fig. 5(A4)). In all graphs, CHO-K1, the CFTR-free cell type, or negative control, is represented with blue color derivatives, while the CHO-CFTR population for which CFTR is fully functional is symbolized in red tones. The CHO-ΔF508 and CHO-G551D cell strains, expressing two CFTR mutated, are depicted with a variation of yellow and green respectively. As described in Section 2.5, the four variants CHO cells are perfused in bath medium during 5 min before transient application of 8Br-cAMP at 1 mM for 5 min (grey boxes in Figs. 5(B)-(F)). Then, cells are rinsed during 15 min. The 8Br-cAMP application, through the action to open the CFTR channel's gate, induces a Cl^- exit accompanied for osmotic reasons by a water efflux, which consistently results in a strong QPS increase [6].

In cells exempt of functional CFTR protein (CHO-K1), the weak QPS response is due to a small water exit following the drug exposure (blue curve, Fig. 5(B)). In contrast, CHO-CFTR exhibits a quick and strong QPS increase due to the activation of the CFTR protein leading again to a substantial water efflux (red curve, Fig. 5(B)). The two other CHO cell lines expressing mutated CFTR variants, exhibit weak QPS responses (green curve, CHO-G551D and yellow curve, CHO-ΔF508del in Fig. 5(B)), with profiles remarkably close to those obtained for CHO-K1 cells (CFTR-free) thus stressing a defective CFTR activity. Consistently the application of forskolin (10 µM, 5 min), a direct activator of the adenylate cyclase, induces on the four cultures results like those of 8Br-cAMP (data not shown).

Similarly to neurons viability experiments, whether environmental differences are likely to affect the cell cultures of the four coverslip areas delimited by the insert is assessed. For this purpose, a stimulation with the 8Br-cAMP in two different configurations (A-configuration, and B-configuration) corresponding to two orientations of the coverslip within the fluidic device (Figs. 5(C)-(F)) is applied. For any of the four cell types, regardless the configuration used, no significant differences in 8Br-cAMP-mediated QPS reponses could be measured (Student's t-tests, $p \geq 0.23$ to 0.95). These results stress that, within the fluidic device, the four coverslip regions

Optics EXPRESS

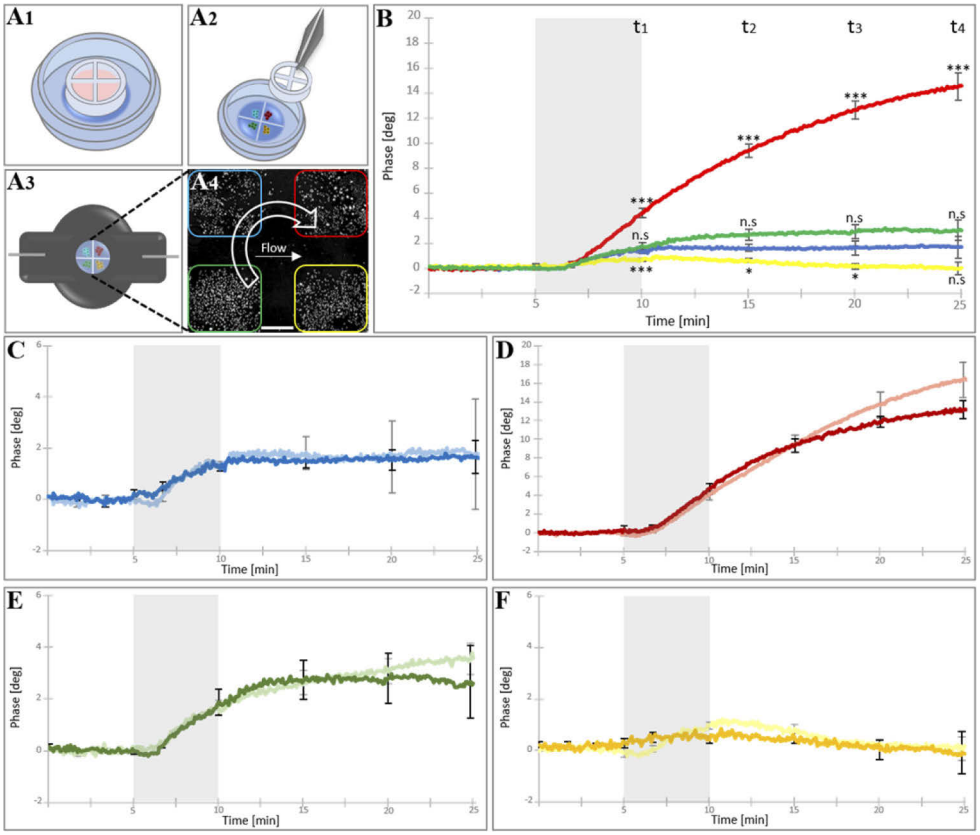

Fig. 5. Cellular multiplexing in the fluidic device. For all graphs, the colors are attributed as follows: the CHO-K1 cells are represented in blue; the CHO-CFTR population are in red; then the CHO-G551D and CHO-ΔF508 are respectively in green and yellow colors. The two explored positions of the distinct cultures in the fluidic device correspond to two orientations, at 180 degrees to each other, of the coverslip. (A1) Culture dish containing the coverslip with the 4-well insert to create independent cell cultures. (A2) Gentle removal of the 4-well insert from the coverslip. To prevent cells from drying, a drop of perfusion medium is placed on top. (A3) Fluidic device with the four CHO cell lines. (A4) Typical quantitative-phase image representing a magnified view of cell culture arrangement in the fluidic device. This image corresponds to the A-orientation where the white arrow indicating the flow direction and the white turning arrow the 180-degree rotation to switch from one configuration to the other (B-configuration). Scale bar represents 500 µm. (B) The QPS time courses of the four CHO cell populations in the A-orientation. These QPS curves were recorded over three time periods, namely before, after, and during 8Br-cAMP exposure (grey box). The QPS curves are extracted from the average of seven independent experiments (number of cells: CHO-K1 $n_{cell} = 352$; CHO-CFTR $n_{cell} = 331$; CHO-G551D $n_{cell} = 340$; CHO-ΔF508 $n_{cell} = 322$). Student's t-tests (* p-value < 0.05, *** p-value < 0.005, or n.s. p-value ≥ 0.05) were performed at 4 different time points ($t_1 = 10$ min; $t_2 = 15$ min; $t_3 = 20$ min; and $t_4 = 25$ min) to assess the differences measured between the negative control cells (CHO-K1) and cystic fibrosis cell models in response to the application of 8Br-cAMP. (C)-(F) Each graph shows two QPS time courses, before, after, and during 8Br-cAMP exposure, for a single cell population but for the two different orientations of the coverslip. The light colors correspond to 3 independent experiments ($n_{cell} \sim 150$) the performed in the A-configuration and the dark colors to 4 independent experiments ($n_{cell} \sim 187$) performed in the B-configuration.

Optics EXPRESS

delimited by the insert present sufficiently similar environmental conditions to not significantly affect the CHO populations to the point of modifying their responses to 8Br-cAMP. It should be noted that even if any environmental effects from these 8Br-cAMP stimulation experiments cannot be formally excluded, these results nevertheless represent a strong indication that there are no major environmental effects between these four regions.

4. Conclusion

Unlike the fluidic device presented in [12], characterized by a small field-of-view in the form of a slit and dedicated to obtain fast rinsing to measure cell biophysical parameters, including absolute cell volume, in the present work we have developed a more complex, large field-of-view, low-cost, and 3D-printed fluidic device dedicated to achieve multiplexed monitoring of cell cultures. Specifically, this biocompatible fluidic device was engineered to produce laminar and homogeneous flow over a major part of its extensive imaging cavity. This flow optimization, designed with CFD and verified experimentally with μPIV, involves two-step diffuser and nozzle at the entry and exit of the imaging cavity, respectively. Specifically, it was stressed that the four cultures present in the fluidic device are exposed to remarkably similar environmental conditions, leading to be able to discriminate their intrinsic properties. This was illustrated by simultaneously monitoring the QPS responses of four different CHO cell lines, transfected with different isoforms of the CFTR chloride channel, when stimulated by two different agonists (8Br-cAMP, forskolin). Such stimulations allowed to adequately replicate known QPS responses that reflect cellular water effluxes specific to the different CHO cell lines [6]. The ability to image multiple cell cultures requires a sufficiently large field-of-view, thus limiting the magnification and resolution. The use of a 2.5x-microscope objective with a NA of 0.07 is an interesting choice since it allows to observe 800 to 1200 cells in one shot while keeping the possibility to measure QPS responses at the individual cell level. Moreover, for this type of cellular response elicited by pharmacological compounds, the analysis of a few hundred cells, repeated over two or three experiments, becomes enough to establish a reproducibility of results. The insert dividing the coverslip into four regions thus brings a time saving close to a factor of four in obtaining reproducible data. Considering the microscope objective used, an insert allowing to divide the coverslip in a larger number of regions would not necessarily bring an additional temporal gain knowing that it would contribute to reduce the number of cells observable in a single shot from each region. Finally, this optimized fluidic device allows the design, and use of sophisticated experimental protocols (application of several substances in a transient, concomitant, or sequential manner) conducive to deciphering in details cellular processes or mechanisms and their interrelationships. It is also important to underline that this multiplexed monitoring of cell cultures can also be advantageously applied to other imaging approaches than DHM, and QPI in a more general manner, such as fluorescence live-cell imaging.

Funding. Natural Sciences and Engineering Research Council of Canada (RGPIN-2018-06198); Canada Excellence Research Chairs, Government of Canada; Canada Foundation for Innovation (34265, 36689); Université de Lausanne; Fondation de Préfargier.

Acknowledgments. The authors acknowledge C. Martel and M.-E. Crochetière.

Disclosures. P. Marquet declares a potential conflict as co-founder of Lyncée Tec. However, this independent study was performed in academic laboratories.

Data availability. Data underlying the results presented in this paper are not publicly available at this time but may be obtained from the authors upon reasonable request.

References

1. Y. Park, C. Depeursinge, and G. Popescu, "Quantitative phase imaging in biomedicine," Nat. Photonics **12**(10), 578–589 (2018).
2. L. Kastl, M. Isbach, D. Dirksen, J. Schnekenburger, and B. Kemper, "Quantitative phase imaging for cell culture quality control," Cytom. Part A **91**(5), 470–481 (2017).

Optics EXPRESS

3. T. O'Connor, S. Rawat, A. Markman, and B. Javidi, "Automatic cell identification and visualization using digital holographic microscopy with head mounted augmented reality devices," Appl. Opt. **57**(7), B197–B204 (2018).
4. M. Rubin, O. Stein, N. A. Turko, Y. Nygate, D. Roitshtain, L. Karako, I. Barnea, R. Giryes, and N. T. Shaked, "TOP-GAN: Stain-free cancer cell classification using deep learning with a small training set," Med. Image Anal. **57**, 176–185 (2019).
5. P. Jourdain, N. Pavillon, C. Moratal, D. Boss, B. Rappaz, C. Depeursinge, P. Marquet, and P. J. Magistretti, "Determination of Transmembrane Water Fluxes in Neurons Elicited by Glutamate Ionotropic Receptors and by the Cotransporters KCC2 and NKCC1: A Digital Holographic Microscopy Study," J. Neurosci. **31**(33), 11846–11854 (2011).
6. P. Jourdain, F. Becq, S. Lengacher, C. Boinot, P. J. Magistretti, and P. Marquet, "The human CFTR protein expressed in CHO cells activates aquaporin-3 in a cAMP-dependent pathway: study by digital holographic microscopy," J. Cell Sci. **127**, 546–556 (2013).
7. B. Rappaz, P. Jourdain, D. Banfi, F. Kuttler, P. Marquet, and G. Turcatti, "Image-Based Marker-Free Screening of GABA A Agonists, Antagonists, and Modulators," SLAS Discov. Adv. Sci. Drug Discov. **25**(5), 458–470 (2020).
8. K. H. Bleicher, H.-J. Böhm, K. Müller, and A. I. Alanine, "Hit and lead generation: beyond high-throughput screening," Nat. Rev. Drug Discovery **2**(5), 369–378 (2003).
9. K. P. Mishra, L. Ganju, M. Sairam, P. K. Banerjee, and R. C. Sawhney, "A review of high throughput technology for the screening of natural products," Biomed. Pharmacother. **62**(2), 94–98 (2008).
10. P. Horvath, N. Aulner, M. Bickle, A. M. Davies, E. Del Nery, D. Ebner, M. C. Montoya, P. Östling, V. Pietiäinen, L. S. Price, S. L. Shorte, G. Turcatti, C. von Schantz, and N. O. Carragher, "Screening out irrelevant cell-based models of disease," Nat. Rev. Drug Discovery **15**(11), 751–769 (2016).
11. B. R. Munson, D. F. Young, T. H. Okiishi, and W. W. Huebsch, *Fundamentals of fluid mechanics*, 6th ed. (Wiley, 2009).
12. E. Bélanger, S. A. Lévesque, É. Rioux-Pellerin, P. Lavergne, and P. Marquet, "Measuring Absolute Cell Volume Using Quantitative-Phase Digital Holographic Microscopy and a Low-Cost, Open-Source, and 3D-Printed Flow Chamber," Front. Phys. **7**, 172 (2019).
13. K. Alessandri, L. Andrique, M. Feyeux, A. Bikfalvi, P. Nassoy, and G. Recher, "All-in-one 3D printed microscopy chamber for multidimensional imaging, the UniverSlide," Sci. Rep. **7**(1), 42378 (2017).
14. J. D. Wardyn, C. Sanderson, L. E. Swan, and M. Stagi, "Low cost production of 3D-printed devices and electrostimulation chambers for the culture of primary neurons," J. Neurosci. Methods **251**, 17–23 (2015).
15. A. L. Tyson, S. T. Hilton, and L. C. Andreae, "Rapid, simple and inexpensive production of custom 3D printed equipment for large-volume fluorescence microscopy," Int. J. Pharm. **494**(2), 651–656 (2015).
16. L. Csanády, P. Vergani, and D. C. Gadsby, "Structure, gating, and regulation of the CFTR anion channel," Physiol. Rev. **99**(1), 707–738 (2019).
17. COMSOL Multiphysics, CFD Module User's Guide v5.6 (2020).
18. J.-Y. Tinevez, N. Perry, J. Schindelin, G. M. Hoopes, G. D. Reynolds, E. Laplantine, S. Y. Bednarek, S. L. Shorte, and K. W. Eliceiri, "TrackMate: An open and extensible platform for single-particle tracking," Methods **115**, 80–90 (2017).
19. S. A. Lévesque, J. M. Mugnes, E. Bélanger, and P. Marquet, "Sample and substrate preparation for exploring living neurons in culture with quantitative-phase imaging," Methods **136**, 90–107 (2018).
20. L. Bulteau, R. Dérand, Y. Mettey, T. Métayé, M. R. Morris, C. M. McNeilly, C. Folli, L. J. V. Galietta, O. Zegarra-Moran, M. M. C. Pereira, C. Jougla, R. L. Dormer, J.-M. Vierfond, M. Joffre, and F. Becq, "Properties of CFTR activated by the xanthine derivative X-33 in human airway Calu-3 cells," Am. J. Physiol. Physiol. **279**(6), C1925–C1937 (2000).
21. R. Dérand, L. Bulteau-Pignoux, Y. Mettey, O. Zegarra-Moran, L. D. Howell, C. Randak, L. J. V. Galietta, J. A. Cohn, C. Norez, L. Romio, J.-M. Vierfond, M. Joffre, and F. Becq, "Activation of G551D CFTR channel with MPB-91: regulation by ATPase activity and phosphorylation," Am. J. Physiol. Physiol. **281**(5), C1657–C1666 (2001).
22. E. Bélanger, J.-P. Bérubé, B. de Dorlodot, P. Marquet, and R. Vallée, "Comparative study of quantitative phase imaging techniques for refractometry of optical waveguides," Opt. Express **26**(13), 17498–17511 (2018).
23. P. Marquet, B. Rappaz, P. J. Magistretti, E. Cuche, Y. Emery, T. Colomb, and C. Depeursinge, "Digital holographic microscopy: a noninvasive contrast imaging technique allowing quantitative visualization of living cells with subwavelength axial accuracy," Opt. Lett. **30**(5), 468–470 (2005).
24. E. Bélanger, S. A. Lévesque, G. Anctil, A.-S. Poulin-Girard, and P. Marquet, "Low-cost production and sealing procedure of mechanical parts of a versatile 3D-printed perfusion chamber for digital holographic microscopy of primary neurons in culture," Proc. SPIE **10074**, 100741S (2017).